

ON THE COMPLETENESS OF THE SET OF RADIAL TREFFTZ FUNCTIONS USED BY THE BKM IN THE SOLUTION OF VISCOELASTICITY PROBLEMS

Alfredo Canelas^a and Berardi Sensale^b

^a*Instituto de Estructuras y Transporte, Facultad de Ingeniería, UdelaR, J. Herrera y Reissig 565,
CP 11300, Montevideo, Uruguay, acanelas@fing.edu.uy, <http://www.fing.edu.uy/~acanelas>*

^b*Instituto de Estructuras y Transporte, Facultad de Ingeniería, UdelaR, J. Herrera y Reissig 565,
CP 11300, Montevideo, Uruguay, sensale@fing.edu.uy*

Keywords: Boundary Knot Method, Viscoelasticity, Trefftz functions.

Abstract. The Boundary Knot Method (BKM) is a truly meshless, RBF-based method which has been used to solve many problems in mathematical physics and engineering, like the Helmholtz problem, plate vibration, Poisson, convection-diffusion, eigenanalysis in Acoustics, etc. In a recent work, the BKM has been applied to two-dimensional harmonic elasticity and viscoelasticity problems. In this paper, a new BKM representation is obtained by means of the Cauchy-Kovalevski-Somigliana solution of the displacements. The completeness of the BKM representations for elasticity and viscoelasticity problems is studied theoretically and numerically.

1 INTRODUCTION

Meshfree methods for the solution of partial differential equations have gained large attention in recent years. These methods avoid the computational effort associated to the mesh generation in mesh-based methods like FEM or BEM. For high dimensional complex-shaped problems, the mesh generation process is usually very time consuming, especially for problems where remeshing is necessary, e.g., for accuracy reasons or when the application requires moving boundaries, like in dynamic free-boundary problems or in shape optimization.

Radial basis functions (RBF) are a general and powerful tool in multi-variable approximation (Buhmann, 2003). Using a particular radial solution of the governing equation (from now on called radial Trefftz function) we can define a specialized RBF method that, in conjunction with the collocation technique, constitutes a truly meshless method, since it only needs a set of distinct centers in the boundary of the domain to build the solution.

The first studied of such RBF-based methods is the well-known method of fundamental solutions (MFS) introduced by Kupradze (1964). It has been recognized as being highly accurate and fast convergent. However, it requires to set a controversial artificial boundary outside the physical domain (Alves, 2009; Cisilino and Sensale, 2002). In recent years, some techniques that avoid the use of the artificial boundary were proposed. For instance, the boundary knot method (BKM), introduced by Kang et al. (1999) and by Chen and Tanaka (2002). The BKM has been used to solve many problems in mathematical physics and engineering, like plate vibration (Kang and Lee, 2001), Poisson (Chen et al., 2005), inhomogeneous Helmholtz (Jin and Zheng, 2005), etc.

In a recent work, the BKM has been applied to two-dimensional elasticity and viscoelasticity problems (Canelas and Sensale, 2010). However, a theorem showing the completeness of the BKM representation for viscoelasticity problems has not been presented yet. With the purpose to obtain a complete representation, a new basis for the solution is obtained here by means of the Cauchy-Kovalevski-Somigliana solution of the displacements (Gurtin, 1972). Assuming that the scalar BKM can represent any solution of the scalar Helmholtz problem, the new basis should be capable to represent any solution of the viscoelasticity problem for the same domain.

The governing equation of harmonic elasticity and viscoelasticity problems is presented in Section 2. Section 3 describes the BKM for the solution of these problems. The new basis is presented in Section 4. The performance of the BKM using the new basis is studied considering some examples presented in Section 5. Finally, the conclusions of this work are presented in Section 6.

2 THE ELASTODYNAMICS EQUATION

The general form of the elastodynamics governing equation for viscoelastic materials in the time domain is (Christensen, 1982)

$$c_P^2(t, \cdot) * \nabla \nabla \cdot \mathbf{u}(x, \cdot) - c_S^2(t, \cdot) * \nabla \times \nabla \times \mathbf{u}(x, \cdot) + \mathbf{b}(x, t) = \ddot{\mathbf{u}}(x, t), \quad (1)$$

where ‘*’ denotes the viscoelastic operator:

$$f(t, \cdot) * g(\cdot) = \int_{\tau_0}^t f(t, \tau) \frac{\partial g}{\partial \tau}(\tau) d\tau, \quad (2)$$

$\mathbf{u}(x, t)$ is the displacement field at point x and time t , $\mathbf{b}(x, t)$ is the body force, and, for the synchronous approximation (Pipkin, 1972; Sensale et al., 2001),

$$\bar{c}_P^2(t, \cdot)^* = \frac{1 - \nu}{(1 + \nu)(1 - 2\nu)\rho} R_E(t, \cdot)^* \quad \text{and} \quad (3)$$

$$\bar{c}_S^2(t, \cdot)^* = \frac{1}{2(1 + \nu)\rho} R_E(t, \cdot)^*, \quad (4)$$

are, respectively, the square of the P-wave velocity and the square of the S-wave velocity in the viscoelastic case, ν is the Poisson ratio, ρ is the density and $R_E(t, \cdot)$ is the relaxation function of the material (Christensen, 1982).

For time-harmonic problems, a description of the governing equation is achieved by applying the Fourier transform to the general equation in the time-domain. For zero body forces, the result may be written as:

$$\bar{c}_P^2(\omega) \nabla \nabla \cdot \bar{\mathbf{u}}(x, \omega) - \bar{c}_S^2(\omega) \nabla \times \nabla \times \bar{\mathbf{u}}(x, \omega) + \omega^2 \bar{\mathbf{u}}(x, \omega) = 0, \quad (5)$$

where ω is the angular frequency, the bar over the displacement vector denotes the transformed variable and

$$\bar{c}_P^2(\omega) = \frac{1 - \nu}{(1 + \nu)(1 - 2\nu)\rho} E^*(\omega), \quad (6)$$

$$\bar{c}_S^2(\omega) = \frac{1}{2(1 + \nu)\rho} E^*(\omega), \quad (7)$$

where $E^*(\omega)$ is the Fourier transform of $R_E(t, \cdot)$, and is known as the complex modulus (Pipkin, 1972; Sensale et al., 2001). Fractional Boltzmann or Kelvin models can be used to define $E^*(\omega)$, see (Schmidt and Gaul, 2002; Canelas and Sensale, 2010). In this paper, the following model is used to define the complex modulus:

$$E^*(\omega) = (1 + 2i\beta)E, \quad (8)$$

where E is the Young modulus of the material and β is known as the viscous damping factor.

3 THE BOUNDARY KNOT METHOD

The starting point in any Trefftz approach is the approximation of the variable of interest, in this case the displacement field, by a superposition of a finite number of functions, each of them solution of the homogeneous governing equation. For the harmonic viscoelastic problem, the approximation \mathbf{u}_N of the displacement field $\bar{\mathbf{u}}$ in the proposed method is

$$\mathbf{u}_N(x, \omega) = \sum_{j=1}^N \hat{\mathbf{u}}(x, x_j, \omega) \boldsymbol{\alpha}_j, \quad (9)$$

where x is a point in the domain Ω of the problem and the N points x_j are fixed sources located in the boundary $\partial\Omega$. The Trefftz function $\hat{\mathbf{u}}$, that provides a matrix of size 2×2 in the two-dimensional problem, has radial symmetry with respect to the source x_j , i.e., $\hat{\mathbf{u}}(x, x_j, \omega) = \hat{\mathbf{u}}(r, \omega)$ where $r = \|x - x_j\|$. The expression of $\hat{\mathbf{u}}$ is described in Section 4. The vectors $\boldsymbol{\alpha}_j$ are the unknowns of the method.

As well as the radial Trefftz functions, \mathbf{u}_N satisfies Eq. (5), i.e.,

$$\bar{c}_P^2(\omega)\nabla\nabla\cdot\mathbf{u}_N(x,\omega)-\bar{c}_S^2(\omega)\nabla\times\nabla\times\mathbf{u}_N(x,\omega)+\omega^2\mathbf{u}_N(x,\omega)=0. \quad (10)$$

Various alternatives exist for imposing the boundary conditions. In the collocation approach, we require the satisfaction of the following equations:

$$\mathbf{u}_N(x_j,\omega)=\tilde{\mathbf{u}}(x_j,\omega), \quad \forall x_j\in\partial\Omega_{\mathbf{u}}, \quad (11)$$

$$\mathbf{p}_N(x_j,\omega)=\tilde{\mathbf{p}}(x_j,\omega), \quad \forall x_j\in\partial\Omega_{\mathbf{p}}, \quad (12)$$

where the left hand sides of Eqs. (11) and (12) are the approximation of the displacement as given in Eq. (9) and its associated traction force. The right hand sides of Eqs. (11) and (12) represent the known boundary conditions. Equations (11) and (12) may be written using Eq. (9) as:

$$\sum_{j=1}^N\mathbf{K}_{ij}\boldsymbol{\alpha}_j=\mathbf{y}_i \quad \Leftrightarrow \quad \mathbf{K}\boldsymbol{\alpha}=\mathbf{y}, \quad (13)$$

where $\boldsymbol{\alpha}_j$ contains the unknowns coefficients of the j^{th} term of the expansion of Eq. (9), $\mathbf{K}_{ij}=\hat{\mathbf{u}}(x_i,x_j,\omega)$ and $\mathbf{y}_i=\tilde{\mathbf{u}}(x_i,\omega)$ if $x_i\in\partial\Omega_{\mathbf{u}}$, and $\mathbf{K}_{ij}=\hat{\mathbf{p}}(x_i,x_j,\omega)$ and $\mathbf{y}_i=\tilde{\mathbf{p}}(x_i,\omega)$ if $x_i\in\partial\Omega_{\mathbf{p}}$. The BKM solves the linear system of Eq. (13) to obtain the approximate solution given by Eq. (9).

4 RADIAL TREFFTZ FUNCTIONS

The expression of the radial Trefftz function proposed by Canelas and Sensalé (2010) in index notation is

$$\hat{\mathbf{u}}_{\ell k}=\frac{1}{2\pi\rho\bar{c}_S^2}\left[\psi\delta_{\ell k}-\chi\frac{\partial r}{\partial x_\ell}\frac{\partial r}{\partial x_k}\right], \quad (14)$$

where the functions ψ and χ are

$$\psi(r)=r^{-2}\left[k_P r J_1(k_P r)-k_S r J_1(k_S r)+k_S^2 r^2 J_0(k_S r)\right], \quad (15)$$

$$\chi(r)=r^{-2}\left[2k_P r J_1(k_P r)-k_P^2 r^2 J_0(k_P r)-2k_S r J_1(k_S r)+k_S^2 r^2 J_0(k_S r)\right], \quad (16)$$

where $r=\|x-x_j\|$, the wave numbers are $k_P=\omega/\bar{c}_P(\omega)$, $k_S=\omega/\bar{c}_S(\omega)$, and J_ν denotes the Bessel function of the first kind and order ν . The traction corresponding to the radial Trefftz function of Eq. (14) on a plane of normal \mathbf{n} is

$$\hat{\mathbf{p}}_{\ell k}=\frac{1}{2\pi}\left[\left(\frac{\partial\psi}{\partial r}-\frac{\chi}{r}\right)\left(\delta_{\ell k}\frac{\partial r}{\partial\mathbf{n}}+\mathbf{n}_\ell\frac{\partial r}{\partial x_k}\right)-\frac{2\chi}{r}\frac{\partial r}{\partial x_\ell}\left(\mathbf{n}_k-2\frac{\partial r}{\partial x_k}\frac{\partial r}{\partial\mathbf{n}}\right)-2\frac{\partial\chi}{\partial r}\frac{\partial r}{\partial x_\ell}\frac{\partial r}{\partial x_k}\frac{\partial r}{\partial\mathbf{n}}+\mathbf{n}_k\left(\frac{\bar{c}_P^2}{\bar{c}_S^2}-2\right)\left(\frac{\partial\psi}{\partial r}-\frac{\partial\chi}{\partial r}-\frac{\chi}{r}\right)\frac{\partial r}{\partial x_\ell}\right]. \quad (17)$$

The radial Trefftz function of Eq. (14) has been found effective to represent the solution of several problems considering simple-connected domains (Canelas and Sensalé, 2010). However, a theorem showing the completeness of the representation of Eq. (9) has not been stated yet. By reason of the large numerical experience accumulated in last years using the scalar BKM for Helmholtz problems, it should be of main importance to prove that the representation of

Eq. (9) is complete whenever the representation used by the BKM for scalar Helmholtz problems is. Unfortunately, the technique employed in (Canelas and Sensale, 2010) to derive the radial Trefftz function of Eq. (14) does not provide for a direct way to prove that.

The object of this section is to obtain a radial Trefftz function capable to represent an approximation of the solution of a viscoelasticity problem providing that the scalar BKM representation is complete for a scalar Helmholtz problem with the same domain. This radial Trefftz function is obtained here by means of the Cauchy-Kovalevski-Somigliana solution of the displacements. The completeness of the Cauchy-Kovalevski-Somigliana solution in the case of harmonic problems and for zero body forces is stated in the next theorem.

Theorem Let \mathbf{u} be a class C^6 solution of Eq. (5) in the open domain Ω that is also continuous in $\bar{\Omega}$. Then, there exist a class C^4 vector field \mathbf{g} such that the following equations hold:

$$\bar{c}_S^2(\omega)\nabla\nabla \cdot \mathbf{g}(x, \omega) - \bar{c}_P^2(\omega)\nabla \times \nabla \times \mathbf{g}(x, \omega) + \omega^2\mathbf{g}(x, \omega) = \mathbf{u}(x, \omega), \quad (18)$$

$$(\bar{c}_S^2(\omega)\nabla \cdot \nabla + \omega^2)(\bar{c}_P^2(\omega)\nabla \cdot \nabla + \omega^2)\mathbf{g}(x, \omega) = 0. \quad (19)$$

Proof: See (Gurtin, 1972) for a demonstration of the previous theorem in the more general framework of non-harmonic elastodynamics.

Let \mathbf{u} be the solution of the problem defined by Eq. (5) in the open domain Ω , and certain boundary conditions on $\partial\Omega$. Assuming that the solution of this problem is regular enough, the previous theorem ensures that there exist a vector field satisfying Eq. (19) that provides the displacement field \mathbf{u} by means of Eq. (18).

Let \mathbf{h} be the vector field defined in Ω by:

$$\mathbf{h}(x, \omega) = (\bar{c}_P^2(\omega)\nabla \cdot \nabla + \omega^2)\mathbf{g}(x, \omega). \quad (20)$$

From Eq. (19), the vector field \mathbf{h} satisfies the following equation:

$$(\bar{c}_S^2(\omega)\nabla \cdot \nabla + \omega^2)\mathbf{h}(x, \omega) = 0. \quad (21)$$

It is worth mentioning that the Cauchy-Kovalevski-Somigliana solution of the displacement field is not unique. In fact, there exist infinite solutions \mathbf{g} of Eqs. (18)-(19). For the same reason the vector field \mathbf{h} is not unique. However, any solution \mathbf{h} derived from Eq. (20) is a solution of (21) and, as Eq. (21) decouples in three scalar Helmholtz equations, the vector field \mathbf{h} can be approximated using the scalar BKM approach (Kang et al., 1999; Chen and Tanaka, 2002). That is, choosing N sources on the boundary of Ω , an approximation \mathbf{h}_N for \mathbf{h} can be represented by:

$$\mathbf{h}_N(x, \omega) = \sum_{j=1}^N \hat{\varphi}_S(x, x_j, \omega)\boldsymbol{\alpha}_j. \quad (22)$$

In the two-dimensional problem, the 2×2 matrix field $\hat{\varphi}_S = \hat{\varphi}_S\mathbf{I}$, where \mathbf{I} is the identity matrix and $\hat{\varphi}_S$ is the radial Trefftz function of the scalar BKM, $\hat{\varphi}_S(x, x_j, \omega) = J_0(k_S r)$.

To obtain an approximate solution for \mathbf{g} we observe that it is a solution of the non-homogeneous problem defined by Eq. (20). Thus, the idea proposed here to construct the approximate solution for \mathbf{g} is the following. As an approximation of the particular solution of the Eq. (20) we take an exact particular solution for the approximated body forces \mathbf{h}_N . Then, we add the general representation of the BKM approximation of the homogeneous solution obtained considering

the same sources as for \mathbf{h}_N . A direct differentiation shows that an exact particular solution \mathbf{g}_N^p for the approximated body forces \mathbf{h}_N is

$$\mathbf{g}_N^p(x, \omega) = \sum_{j=1}^N (k_P^2 - k_P^2)^{-1} \hat{\varphi}_S(x, x_j, \omega) \boldsymbol{\alpha}_j. \quad (23)$$

Redefining the parameters $\boldsymbol{\alpha}_j$ taking into account the constant factor $(k_P^2 - k_P^2)^{-1}$, and adding the homogeneous solution, the BKM approximation for \mathbf{g} is

$$\mathbf{g}_N(x, \omega) = \sum_{j=1}^N \hat{\varphi}_S(x, x_j, \omega) \boldsymbol{\alpha}_j + \sum_{j=1}^N \hat{\varphi}_P(x, x_j, \omega) \boldsymbol{\beta}_j. \quad (24)$$

where $\hat{\varphi}_P = \varphi_P \mathbf{I}$, and $\hat{\varphi}_P(x, x_j, \omega) = J_0(k_P r)$.

Coming back to the displacements, Eq. (18) gives the following approximation:

$$\mathbf{u}_N(x, \omega) = \sum_{j=1}^N \hat{\mathbf{u}}_S(x, x_j, \omega) \boldsymbol{\alpha}_j + \sum_{j=1}^N \hat{\mathbf{u}}_P(x, x_j, \omega) \boldsymbol{\beta}_j, \quad (25)$$

where the functions $\hat{\mathbf{u}}_S$ and $\hat{\mathbf{u}}_P$ can be expressed, to within multiplicative constants, by Eq. (14), where in this case ψ and χ must be defined as

$$\psi(r) = r^{-2} [-k_S r J_1(k_S r) + k_S^2 r^2 J_0(k_S r)], \quad (26)$$

$$\chi(r) = r^{-2} [-2k_S r J_1(k_S r) + k_S^2 r^2 J_0(k_S r)], \quad (27)$$

for $\hat{\mathbf{u}}_S$ and

$$\psi(r) = r^{-2} [k_P r J_1(k_P r)], \quad (28)$$

$$\chi(r) = r^{-2} [2k_P r J_1(k_P r) - k_P^2 r^2 J_0(k_P r)], \quad (29)$$

for $\hat{\mathbf{u}}_P$. The surface tractions associated to $\hat{\mathbf{u}}_S$ and $\hat{\mathbf{u}}_P$ are given by Eq. (17), using their respective expressions of ψ and χ .

From Eqs. (15)-(16) and (26)-(29), it can be observed that $\hat{\mathbf{u}} = \hat{\mathbf{u}}_S + \hat{\mathbf{u}}_P$, so that the radial Trefftz function $\hat{\mathbf{u}}$ proposed in (Canelas and Sensalé, 2010) is a sum of $\hat{\mathbf{u}}_S$, a motion of wave number k_S (hence a pure isochoric motion), and $\hat{\mathbf{u}}_P$, a motion of wave number k_P (hence a pure irrotational motion). In addition, this last equality shows that any function of the form given by Eq. (9) can easily be expressed in the form of Eq. (25). Figure 1 shows a graphic representation of the displacements corresponding to the first column of $\hat{\mathbf{u}}_S$ and $\hat{\mathbf{u}}_P$.

A BKM approach similar than the proposed in (Canelas and Sensalé, 2010) can be implemented using the expansion of Eq. (25). The main difference is that the number of collocation points must double the number of source points, since for each source point four unknown parameters are defined.

5 EXAMPLES

We present numerical results obtained for two simple problems, an example considering a circle domain and an example of a square domain. For both examples a broad range of frequencies was considered in the performance evaluation of the BKM. The results obtained are compared to the exact solution. The frequency response modulus and the condition number

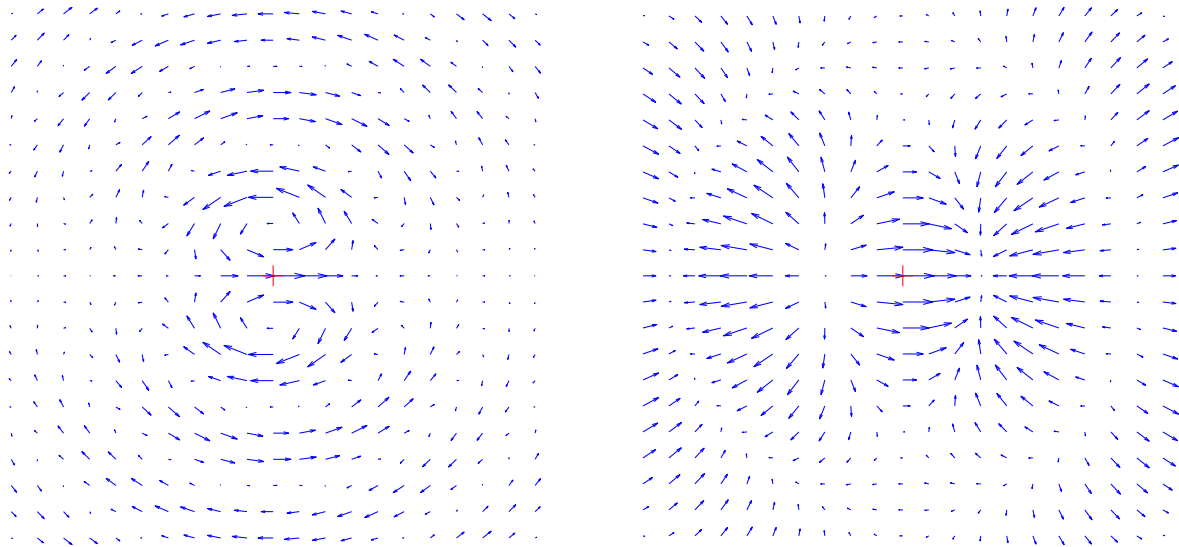


Figure 1: Diagrams showing the displacements corresponding to the first column of the radial Trefftz functions. Left: Isochoric displacement $\hat{\mathbf{u}}_S$. Right: Irrotational displacement $\hat{\mathbf{u}}_P$. Central red pluses: Location of the sources.

of the linear systems are plotted versus the angular frequency, which is normalized by the first natural frequency ω_1 of the pure elastic problem. The exact solutions as well as the first natural frequencies are given in Appendix A.

In all the figures of this section, the BKM approach proposed in (Canelas and Sensale, 2010) (based on the expressions of Eqs. (9), (14) and (15)-(16)) is referenced by BKM-O. The BKM approach proposed here (based on the expressions of Eqs. (25), (14) and (26)-(29)) is referenced by BKM-N.

The implementations of the BKM-O and BKM-N use a double precision floating-point representation of real numbers (machine precision $\approx 10^{-16}$). A standard solver based on Gaussian elimination was used to solve the systems of linear equations. Thus, large numerical errors in the solution of linear systems are expected for condition numbers higher than 10^{16} .

5.1 Circle

In this example, we consider a circle of radius $R = 6.0$ m. The material properties are $G = 1.0 \times 10^6$ Pa, $\nu = 0.25$, $E = 2(1 - \nu)G$, $\beta = 0.05$ and $\rho = 100.0$ kg/m³.

In the first case, the circle is subject to boundary displacements matching the displacements of the radial Trefftz functions $\hat{\mathbf{u}}_S$ and $\hat{\mathbf{u}}_P$, for a source located at the rightmost point of the circle and for four different values of the angular frequency ω . The purpose of this example is to verify that the BKM approach proposed in (Canelas and Sensale, 2010) is capable to represent accurately each of the functions of the expansion of Eq. (25), at least for the case of a circle domain (the converse is obviously true in view of the equality $\hat{\mathbf{u}} = \hat{\mathbf{u}}_S + \hat{\mathbf{u}}_P$).

Figures 2-3 show the displacements along the horizontal diameter of the circle obtained by the BKM-O compared with the exact solution $\hat{\mathbf{u}}_S$. Figures 4-5 show the same for the exact solution $\hat{\mathbf{u}}_P$. Figures 2- 5 show that the expansion of the BKM-O can represent the functions $\hat{\mathbf{u}}_S$ and $\hat{\mathbf{u}}_P$ for this circle domain problem. Using a mesh of 16 nodes, the BKM-O obtained accurate results for the three lowest frequencies tested, and using a mesh of 32 nodes it obtained accurate results even for the highest frequency.

In the second case, a uniform radial displacement of the boundary of value $U = 1.0$ m is considered. The frequency response modulus at a point on the boundary is given in Fig. 6.

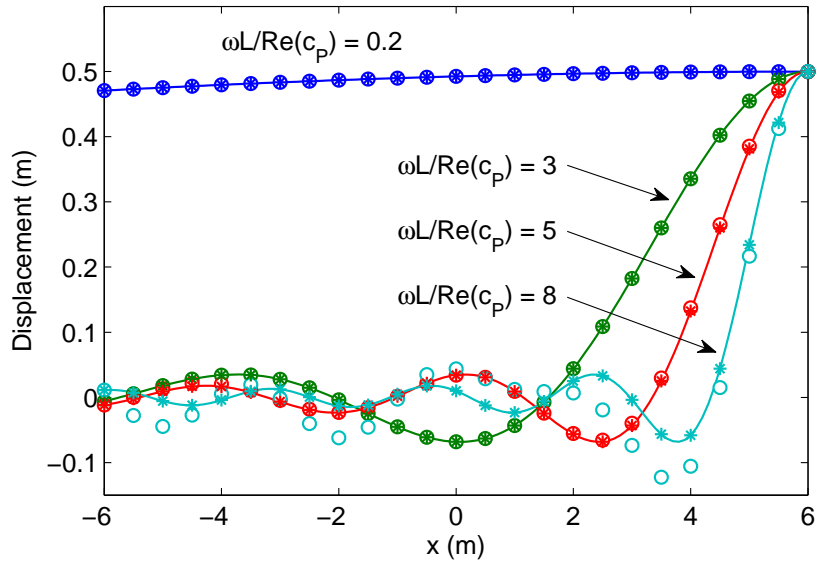


Figure 2: Horizontal displacements along the horizontal diameter of the circle obtained by the BKM-O compared with the exact solution corresponding to the first column of \hat{u}_S . Circles: Mesh of 16 nodes. Stars: Mesh of 32 nodes. Solid line: exact solution.

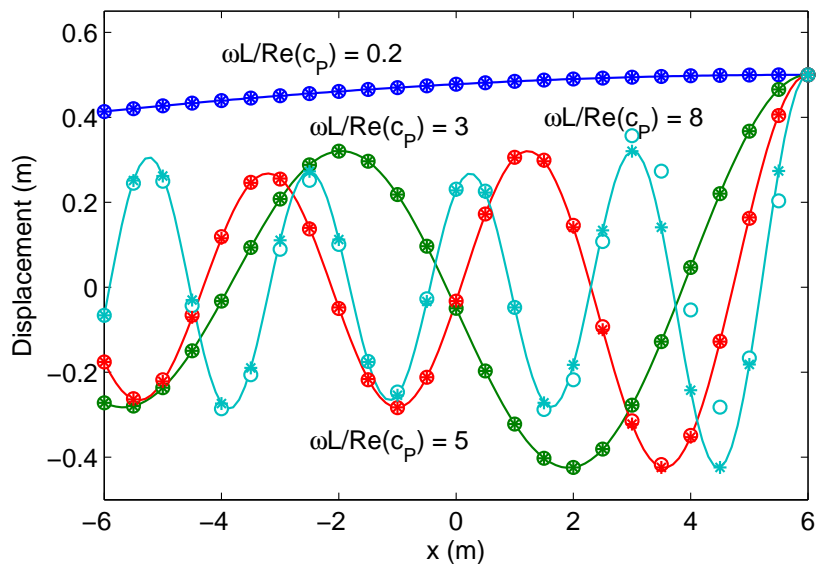


Figure 3: Vertical displacements along the horizontal diameter of the circle obtained by the BKM-O compared with the exact solution corresponding to the second column of \hat{u}_S . Circles: Mesh of 16 nodes. Stars: Mesh of 32 nodes. Solid line: exact solution.

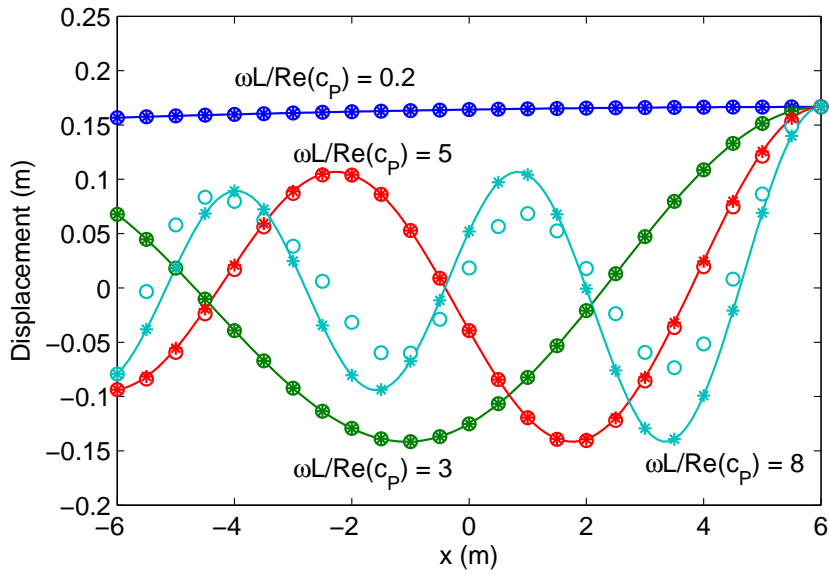


Figure 4: Horizontal displacements along the horizontal diameter of the circle obtained by the BKM-O compared with the exact solution corresponding to the first column of \hat{u}_P . Circles: Mesh of 16 nodes. Stars: Mesh of 32 nodes. Solid line: exact solution.

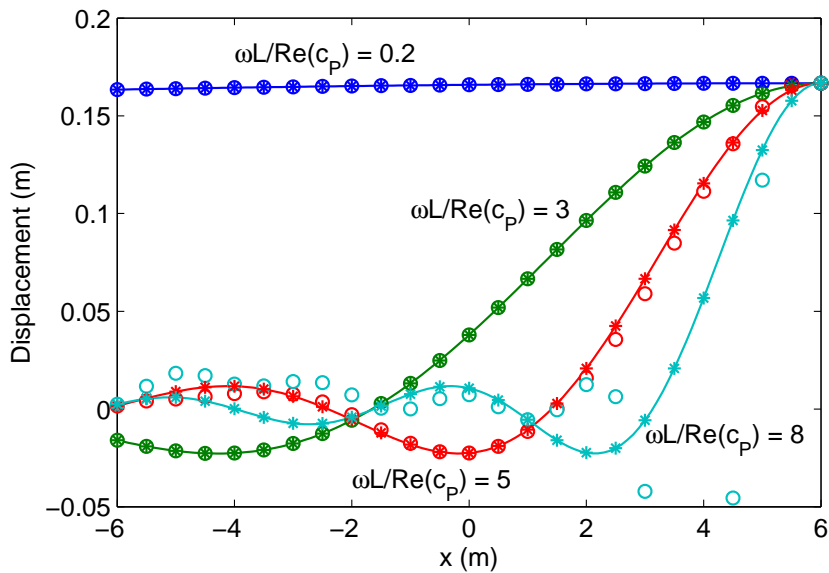


Figure 5: Vertical displacements along the horizontal diameter of the circle obtained by the BKM-O compared with the exact solution corresponding to the second column of \hat{u}_P . Circles: Mesh of 16 nodes. Stars: Mesh of 32 nodes. Solid line: exact solution.

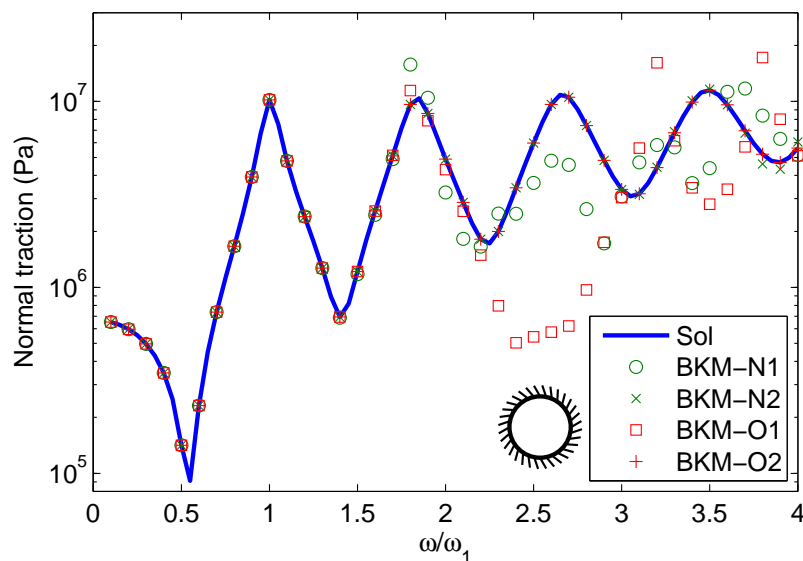


Figure 6: Circle example - Frequency response modulus. Sol: Exact solution, BKM-N1: results of the BKM-N for a mesh of 16 collocation nodes, BKM-N2: results of the BKM-N for a mesh of 32 collocation nodes, BKM-O1: results of the BKM-O for a mesh of 16 collocation nodes, BKM-O2: results of the BKM-O for a mesh of 32 collocation nodes.

Figure 7 shows the condition number of the linear systems. The figures show that the BKM-N and the BKM-O obtain results of similar accuracy. For a mesh of 16 nodes both methods obtain accurate results for frequencies below that of the second peak of the frequency response. For a mesh of 32 nodes, both methods obtain accurate results even till the fourth peak. Figure 7 shows that the linear systems built by the BKM-O are better conditioned than the systems built by the BKM-N.

5.2 Square

The domain of this example consists of a square of side $L = 6.0$ m with mixed boundary conditions: on the bottom side the vertical component of the displacement and the horizontal component of the traction are zero, on the lateral sides the horizontal component of the displacement and the vertical component of the traction are assumed zero, and in the top side there is a uniform normal traction of value $P = 100.0$ Pa. The same material properties as in the Example 5.1 are considered. The closer sources to the corners are located at a distance of one fourth of the mean distance between subsequent sources. The frequency response modulus at the middle point of the top side and the condition number of the linear systems are shown in Figs. 8 and 9, respectively.

As in the previous example, the BKM-N and the BKM-O obtain results of similar accuracy. For a mesh of 16 nodes both methods obtain accurate results for frequencies below that of the third peak of the frequency response. For a mesh of 32 nodes, both methods obtain accurate results for the entire range of tested frequencies. Figure 9 shows that, as in the example above, the linear systems built by the BKM-O are better conditioned than the systems built by the BKM-N.

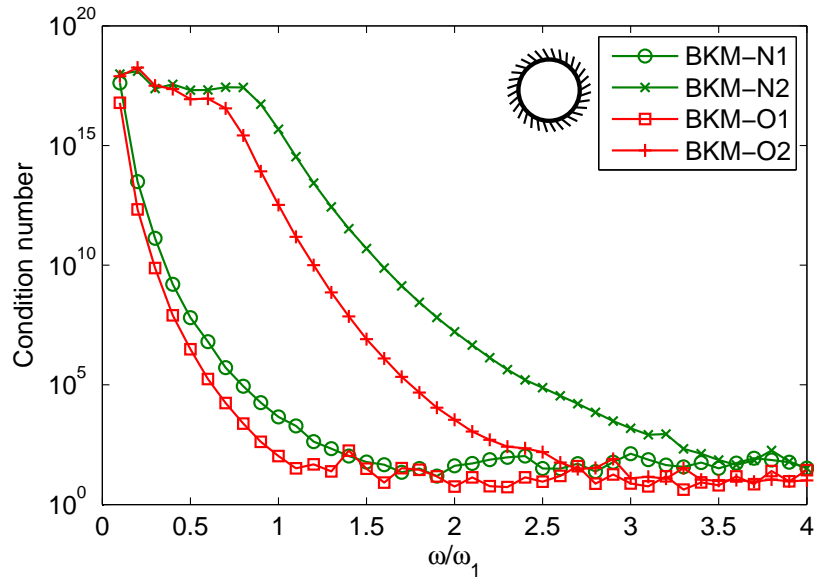


Figure 7: Circle example - Condition number of the linear system. BKM-N1: mesh of 16 collocation nodes, BKM-N2: mesh of 32 collocation nodes. BKM-O1: mesh of 16 collocation nodes, BKM-O2: mesh of 32 collocation nodes.

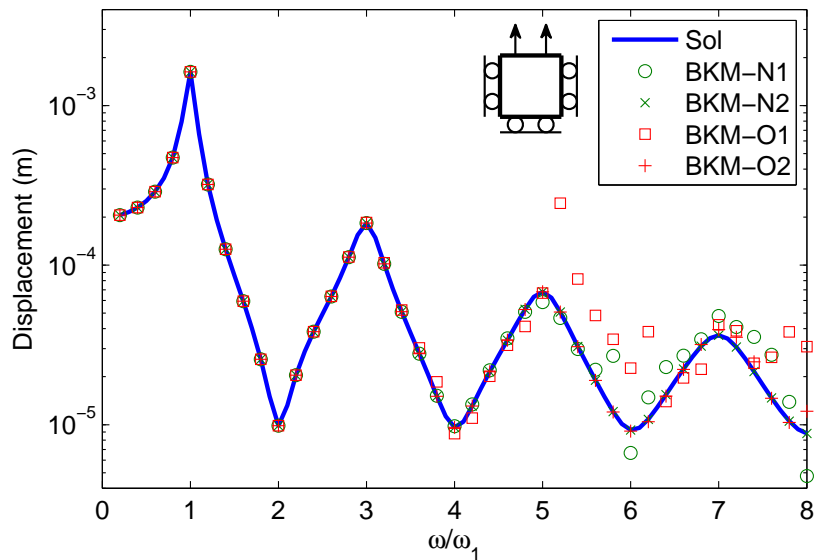


Figure 8: Square example - Frequency response modulus. Sol: Exact solution, BKM-N1: results of the BKM-N for a mesh of 16 collocation nodes, BKM-N2: results of the BKM-N for a mesh of 32 collocation nodes, BKM-O1: results of the BKM-O for a mesh of 16 collocation nodes, BKM-O2: results of the BKM-O for a mesh of 32 collocation nodes.

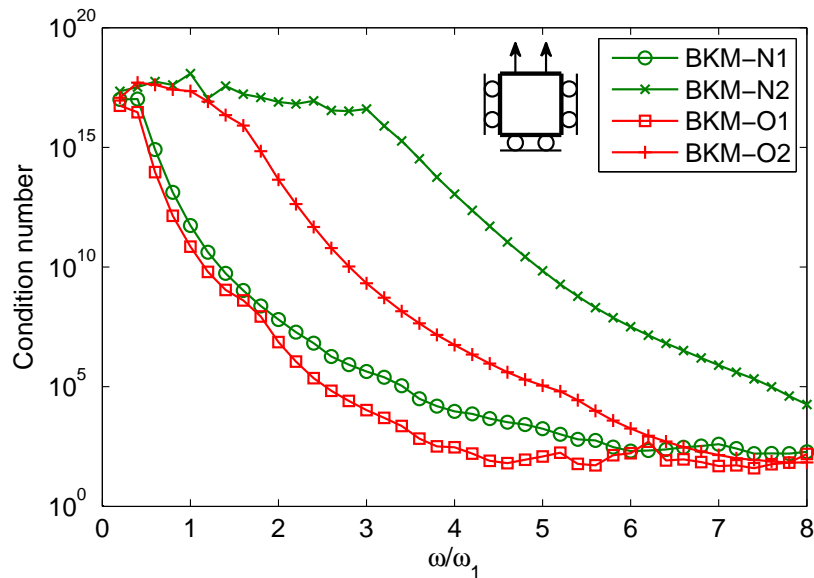


Figure 9: Square example - Condition number of the linear system. BKM-1: mesh of 12 nodes, BKM-2: mesh of 20 nodes.

6 CONCLUSIONS

A new radial Trefftz function for the BKM representation of the solution was obtained by means of the Cauchy-Kovalevski-Somigliana solution of the displacements. The new basis can represent exactly any solution obtained by the BKM using the old basis. In addition, assuming that the scalar BKM can represent any solution of the scalar Helmholtz problem, the new basis should be able to represent any solution of the viscoelasticity problem for the same domain.

Some examples were considered to compare the performance of the BKM using the old and the new set of radial Trefftz functions. For the circle domain problem, it was observed that the old basis could represent the elements of the new basis, so validating the approach presented in (Canelas and Sensale, 2010). The new basis has the extra difficulty of setting more collocation points than source points. In addition, it was observed that the new basis leads to worse conditioned linear systems. Thus, for practical applications the basis presented in (Canelas and Sensale, 2010) is recommended.

ACKNOWLEDGMENT

The authors would like to thank the National Research and Innovation Agency (ANII) of Uruguay for the financial support.

A EXACT SOLUTIONS

The exact solutions for the circle and square problems are presented in Table 1. The scalar constant u_0 must be obtained according to the boundary conditions.

For the circle problem and for an imposed radial displacement of value U :

$$u_0 = U/J_1(\xi), \text{ with:} \quad (30)$$

$$\xi = k_P R. \quad (31)$$

For an imposed radial traction of value P :

$$u_0 = \gamma^2 P \xi^2 / [\rho \omega^2 R (\gamma^2 \xi J_0(\xi) - J_1(\xi))], \text{ with:} \quad (32)$$

$$\gamma = \bar{c}_P / (\sqrt{2} \bar{c}_S), \quad (33)$$

$$\xi = k_P R. \quad (34)$$

For the square problem and for an imposed vertical displacement of value U on the top face:

$$u_0 = U / \sin(\xi), \text{ with:} \quad (35)$$

$$\xi = k_P L. \quad (36)$$

For an imposed vertical traction of value P :

$$u_0 = P \xi / (\rho \omega^2 L \cos(\xi)). \quad (37)$$

The analysis of the exact solutions provides the natural frequencies of the modes excited by the loads considered. They are given in terms of the dimensionless parameter ξ in Tables 2 and 3.

Example	Solution
Circle	$u_0 J_1(k_P r) \mathbf{e}_r$
Square	$u_0 \sin(k_P y) \mathbf{e}_y$

Table 1: Exact solution.

Example	Natural frequencies ^(a)
Circle Dirichlet	$\omega = \bar{c}_P \xi / R, J_1(\xi) = 0$
Circle Neumann	$\omega = \bar{c}_P \xi / R, \gamma^2 \xi J_0(\xi) - J_1(\xi) = 0$
Square Dirichlet	$\omega = \bar{c}_P \xi / L, \sin(\xi) = 0$
Square Neumann	$\omega = \bar{c}_P \xi / L, \cos(\xi) = 0$

(a) Consider the positive solutions of the equations.

Table 2: Natural frequencies.

Example	ξ_1	ξ_2	ξ_3
Circle Dirichlet	3.8317	7.0156	10.173
Circle Neumann ^a	2.0694	5.3957	8.5758
Square Dirichlet	π	2π	3π
Square Neumann	$\pi/2$	$3\pi/2$	$5\pi/2$

(a) For $\gamma \cong 1.2247$.

Table 3: First three natural frequencies.

REFERENCES

Alves C.J.S. On the choice of source points in the method of fundamental solutions. *Eng. Anal. Bound. Elem.*, 33(12):1348–1361, 2009.

- Buhmann M.D. *Radial basis functions: theory and implementations*, volume 12 of *Cambridge Monographs on Applied and Computational Mathematics*. Cambridge University Press, Cambridge, 2003.
- Canelas A. and Sensalé B. A boundary knot method for harmonic elastic and viscoelastic problems using single-domain approach. *Eng. Anal. Bound. Elem.*, 34(10):845–855, 2010.
- Chen W., Shen L.J., Shen Z.J., and Yuan G.W. Boundary knot method for Poisson equations. *Eng. Anal. Bound. Elem.*, 29(8):756–760, 2005.
- Chen W. and Tanaka M. A meshless, integration-free, and boundary-only RBF technique. *Comput. Math. Appl.*, 43(3-5):379–391, 2002.
- Christensen R.M. *Theory of Viscoelasticity, An Introduction*. Academic Press, New York, second edition, 1982.
- Cisilino A.P. and Sensalé B. Application of a simulated annealing algorithm in the optimal placement of the source points in the method of the fundamental solutions. *Comput. Mech.*, 28(2):129–136, 2002.
- Gurtin M.E. The linear theory of elasticity. In *Handbuch der Physik, Volume VIa/2*. Springer-Verlag, Berlin, Heidelberg, New York, 1972.
- Jin B. and Zheng Y. Boundary knot method for some inverse problems associated with the Helmholtz equation. *Internat. J. Numer. Methods Eng.*, 62(12):1636–1651, 2005.
- Kang S.W. and Lee J.M. Free vibration analysis of arbitrarily shaped plates with clamped edges using wave-type functions. *J. Sound Vibration*, 242(1):9–26, 2001.
- Kang S.W., Lee J.M., and Kang Y.J. Vibration analysis of arbitrarily shaped membranes using non-dimensional dynamic influence function. *J. Sound Vibration*, 221(1):117–132, 1999.
- Kupradze V.D. A method for the approximate solution of limiting problems in mathematical physics. *USSR Comput. Math. Math. Phys.*, 4:199–205, 1964.
- Pipkin A.C. *Lectures on Viscoelasticity Theory*. Springer-Verlag, New York, Heidelberg, Berlin, 1972.
- Schmidt A. and Gaul L. Finite element formulation of viscoelastic constitutive equations using fractional time derivatives. *Nonlinear Dyn.*, 29(1–4):37–55, 2002.
- Sensalé B., Partridge P.W., and Creus G.J. General boundary element solution for ageing viscoelastic structures. *Internat. J. Numer. Methods Eng.*, 50(6):1455–1468, 2001.